Optical and Quantum Electronics (2023) 55:321
https://doi.org/10.1007/s11082-023-04541-1

The fabrication processes and simple micro-cavity size adjustment of fiber Mach-Zehnder interferometer by laser-induced micro-plasma

Cai Shuhao[1,2] · Maksim Sergeev[1] · Andrey Petrov[1] · Sergey Varzhel[1] · Li Li[2]

Received: 19 July 2022 / Accepted: 1 January 2023 / Published online: 13 February 2023

Abstract
The detailed fabrication processes of fiber Mach-Zehnder interferometers (FMZIs) by nanosecond laser-induced micro-plasma and its simple micro-cavity size adjustment are proposed and demonstrated. The fabrication can be divided into 4 processes: (1) heat transfer, (2) micro-plasma formation, (3) micro-plasma expansion and ablation, (4) cooling down and micro-structure formation. The simple micro-cavity size adjustment is proposed based on the above understanding, instead of the "point processing" of femtosecond laser, here only the focus position is required to be moved. The fabricated FMZI exhibits a high sensitivity of -15,811 nm/RIU (refractive index unit) for the index sensing application.

Keywords Fiber Mach-Zehnder interferometer · Fabrication processes · Laser-induced micro-plasma · Micro-cavity size adjustment · Refractive index sensing

1 Introduction

Fiber sensors, including fiber Bragg grating (FBG) (Rao 1997; Albert et al. 2013), long period fiber grating (LPFG) (Wang 2010), fiber Fabry-Perot interferometers (Rao et al. 2007; Wei et al. 2008), fiber Mach-Zehnder interferometers (Zhao et al. 2019), fiber Michelson interferometers (Tian et al. 2008), fiber Sagnac interferometers (Chunyang et al. 2014) et al., are intensively studied in the last decades for their sensing capabilities in complicated or hazardous environment. In these sensing systems, the physical, chemical or biological parameters are converted into optical signal, especially optical spectrum by these fiber sensors, leading to immunity to electromagnetic interference. Among these verious fiber sensors, the micro-cavity-based fiber Mach-Zehnder interferometers (FMZIs) have attracted much attention for their ultra-compact sizes (Park et al. 2009; Wang et al. 2009; Shuhao et

✉ Cai Shuhao
caishuhao@mail.ru

[1] ITMO University, 49 Kronverksky av., 197101 St. Petersburg, Russia

[2] School of Electronic and Optical Engineering, Nanjing University of Science and Technology, 210094 Nanjing, China

al. 2021) and high sensitivity (Jiang et al. 2011; Li et al. 2014, 2016, 2017; Sun et al. 2016; Janik et al. 2017; Zhao et al. 2019). Despite their multiple merits, up to present, only 2 methods are proposed in fabricating FMZIs of micro-cavities: femtosecond (fs) laser (Park et al. 2009) and laser-induced micro-plasma (Shuhao et al. 2021).

Femtosecond laser was a unique method and more adopted in fabricating FMZIs of micro-cavities before the method by laser-induced micro-plasma. However, femtosecond laser fabrication system is not always available for fiber sensing groups due to its high budget, meanwhile it requires very high-precision moving platforms (Zhao et al. 2011, 2019; Sun et al. 2016). Furthermore, the size of micro-cavity determines the processing time of femtosecond laser due to its "point processing" property, which requires more time to fabricate the big size micro-cavity and even consumes a lot of time in some cases. Laser-induced micro-plasma possesses an advantage in the great simplified fabrication system, in which only conventional modest fiber nanosecond laser and ordinary moving platform are required (Shuhao et al. 2021). This method comes from (Veiko et al. 2017; Kostyuk et al. 2015), in which transparent fused silica is processed to fabricate different optical devices. In the work (Shuhao et al. 2021), the chemical etching is followed after laser-induced micro-plasma processing, restricting its further applications. Thus, micro-cavity based FMZI fabricated by laser-induced micro-plasma without chemical etching is in urgent demand. In addition, the fabrication details are not clear, especially considering the special fiber-placing-configuration. Furthermore, instead of femtosecond laser "point processing" property, the simplified adjustment of FMZI micro-cavity size possessed by laser-induced micro-plasma for its "wide scanning processing" property is also attractive.

In this work, we present the detailed fabrication processes of FMZI by laser-induced micro-plasma, and the simple micro-cavity size adjustment is also demonstrated based on the fabrication processes. The fiber cylindrical form works as extra lens to focus the laser beam. The fabrication is divided into 4 processes: (1) heat transfer, (2) micro-plasma formation, (3) micro-plasma expansion and ablation, (4) cooling down and micro-structure formation. Based on the fabrication processes discussion, the micro-cavity size adjusted only by the movement of the focus position, meanwhile, the fabrication time is not prolonged. The fabricated FMZIs exhibit a high sensitivity of -15,811 nm/RIU for refractive index sensing applications.

2 The FMZI fabrication

2.1 The fabrication processes

The overall fabrication scheme of FMZI by laser-induced micro-plasma and its experimental steps were explained in the work (Shuhao et al. 2021) following with chemical etching, here, we concentrate on the fabrication processes and the experimental scheme is redrawn to highlight the processing place as illustrated in Fig. 1(a). A piece of single-mode (SM) fiber, Corning SMF-28, is stripped of its coating and placed tightly between a thin fused silica plate and a polished graphite block. The long working distance microscope objective focuses nanosecond laser beam onto the graphite surface, the laser beam propagates through the silica plate and SMF-28 fiber, respectively. When the platform scans along the direction as indicated by red double arrow in Fig. 1(a) at the speed of 0.5 mm/s, the focused

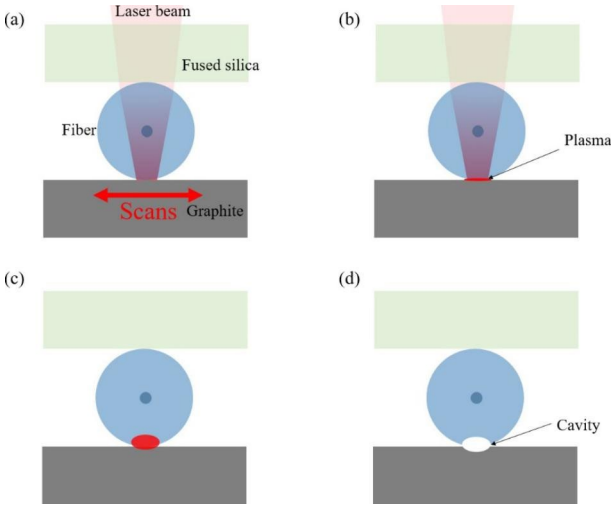

Fig. 1 The FMZI fabrication scheme in the processing place by laser-induced micro-plasma. (a) Heat transfer, (b) micro-plasma formation, (c) micro-plasma expansion and ablation, (d) cooling down and micro-structure formation

laser beam induces the micro-plasma inside the graphite and then ablates the fiber on top. Compared with the other fused silica ablation (Kostyuk et al. 2015; Veiko et al. 2017), here the fiber also serves as a micro-cylindrical lens, which focuses laser beam one more time as illustrated in Fig. 1(a), and the focusing spot on the graphite surface is elliptical rather than circular. This extra focusing power enforces the micro-plasma-ablated in-fiber micro-cavities even deeper.

The nanosecond laser induced micro-plasma in-fiber micro-cavity fabrication can be mainly divided into 4 processes: (1) heat transfer, (2) micro-plasma formation, (3) micro-plasma expansion and ablation, (4) cooling down and micro-structure formation. In the first process of heat transfer as illustrated in Fig. 1(a), the ns laser beam irradiates on the graphite surface, the laser energy transfers to the graphite and meanwhile the heat was also transferred to the fiber from the graphite as the fiber and graphite tightly touched at the beginning of irradiation. Then it continues to the second process, the micro focused area of graphite absorbs huge energy from laser beam, leading to the formation of micro-plasma, which ablates fiber on-top, meanwhile, the laser beam still irradiates as illustrated in Fig. 1(b). Then in the third process, after irradiation of ns laser, the plasma will go on expanding for the plasma continues longer than ns pulse duration (Shuhao et al. 2020) as shown in Fig. 1(c), meanwhile, the plasma will also go on ablating the fiber until the plasma quenched. In the last process, after quenching of the plasma, the graphite and fiber both will cool down, forming stable micro-cavity in fiber and graphite, waiting the next scan as shown in Fig. 1(d). It should be noted that there are three differences between the first scan process and the next one: first, the heat transfer from graphite to fiber can be ignored in the next scan since a micro gap will be ablated between the fiber and graphite after first pulse ablation. Second, the intensity of plasma will gradually become weaker also because of ablated micro gap. Third, the laser beam focusing will be altered due to the cylindrical geometry changing resulted from the ablated micro-cavity in fiber. These concerned factors certainly affect the micro-cavity fabrication, and more investigations are needed for fabrication controlling.

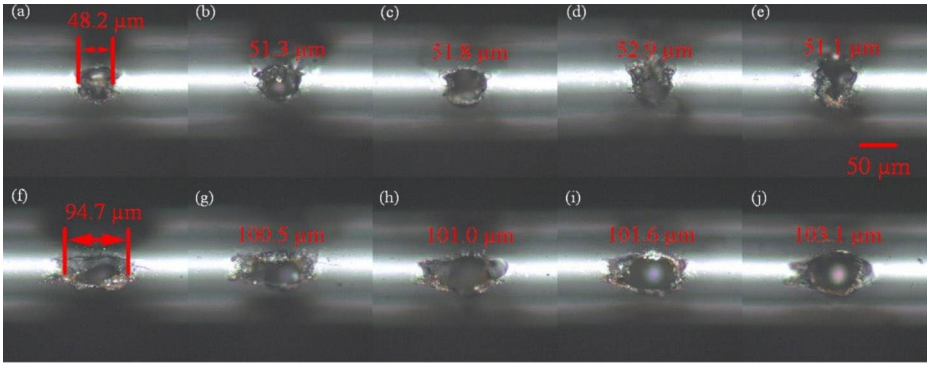

Fig. 2 The open cavity length after 1 to 5 micro-plasma processing scans. (a-e) The graphite surface coincides with the focus plane, the laser power is 8.5 W, and each corresponds to 1 to 5 scans, respectively. (f-j) The graphite surface located higher than the focus plane with 600 μm, the laser power is 14.5 W, and each corresponds to 1 to 5 scans, respectively

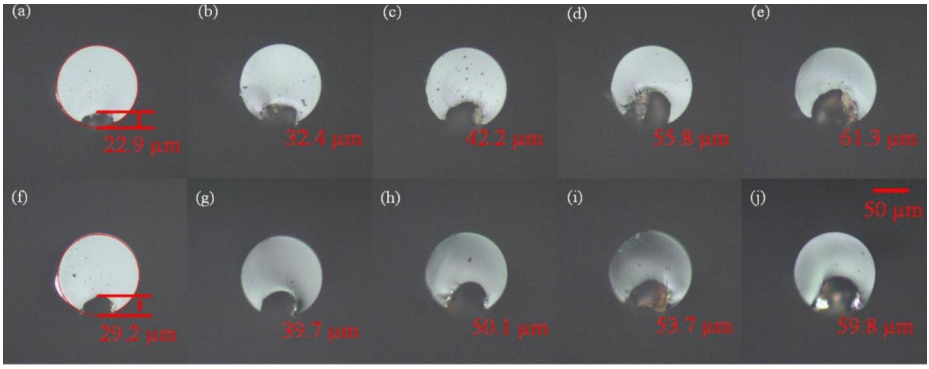

Fig. 3 The micro-cavity depths after 1 to 5 micro-plasma processing scans. (a-e) The graphite surface coincides with the focus plane, the laser power is 8.5 W, and each corresponds to 1 to 5 scans, respectively. (f-j) The graphite surface located higher than the focus plane with 600 μm, the laser power is 14.5 W, and each corresponds to 1 to 5 scans, respectively

2.2 The evolution of micro-cavity

In order to investigate the geometrical evolution of micro-cavity in fiber after each micro-plasma processing scan, the samples are observed by optical microscope. The open cavity lengths are direct measured as illustrated in Fig. 2 (a-j), meanwhile the fiber samples are cut at the deepest area of micro-cavity and the micro-cavity depths are measured from one end face as illustrated in Fig. 3 (a-j). The evolution of open cavity length and micro-cavity depth are drawn in Fig. 4.

As illustrated in Fig. 2 and red polylines in Fig. 4, the open cavity length almost keeps constant after 1 to 5 scans in the same focus condition, as for the graphite surface coincides with the focus plane, the open cavity length keeps around 51 μm, despite the number of scans increases from 1 to 5. Similarly, in the graphite surface located higher than the focus plane with 600 μm, the open cavity length keeps around 101 μm without the influence

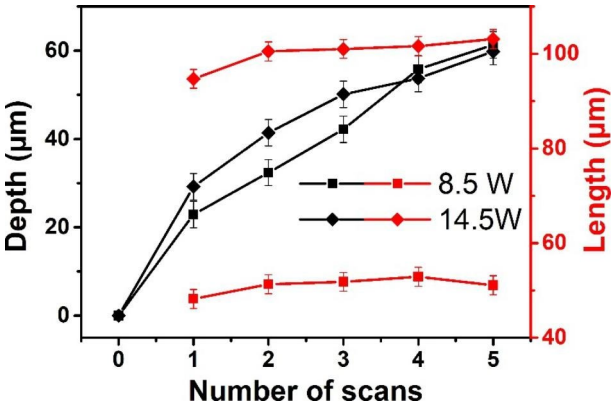

Fig. 4 The evolution of open cavity lengths and micro-cavity depths after micro-plasma processing scans from 1 to 5. The laser power 8.5 and 14.5 W correspond to the graphite surface located in coincidence with focus plane and higher than the focus plane with 600 μm, respectively

of the scanning number. In addition, the all open cavities look like rectangles with some cracks, however these cracks do not affect the final FMZI sensing properties as they located far from the fiber core (Shuhao et al. 2021). The open cavity length is determined by the distance between the graphite surface and focus plane, which will be investigated in details in Sect. 3.

The micro-cavity depth evolves differently from the open cavity length described above. The micro-cavity depth increases as the micro-plasma processing keeps on as illustrated in Fig. 3 and black polylines in Fig. 4. The micro-cavity depth increases mostly after the 1-st micro-plasma processing scan, because no micro gap between graphite and fiber for the 1-st processing as discussed above, resulting in more intensive laser-induced micro-plasma. Later, excluding the randomness of the experiments, the micro-cavity depth goes on increasing with a small tendency to slow down the rising, resulted from the micro gap increasing between the graphite and fiber as discussed above and in the work (Shuhao et al. 2020). It should be noted, firstly, the micro-cavity evolves into more regular crater-like structure as the number of scans more than 4; secondly, after 5 micro-plasma processing scans, the micro-cavity reaches to the fiber core, and in such condition (can be detected by optical spectrum analyzer), less laser power should be utilized to remove less silica in fiber to obtain a well sensitive FMZI.

3 The FMZI micro-cavity size adjustment and sensing

3.1 The adjustment principle and experiment

The experimental scheme for micro-cavity size adjustment is illustrated in Fig. 5. The laser beam focusing size on the graphite surface is determined by the distance d between graphite surface and the focus plane as in Fig. 5, and as micro-plasma processing scans going on, the wider beam size probably produce bigger micro-cavity size. Based on the above principle, the distance from 0 to 600 μm are fixed to fabricate FMZI samples. The fabricated samples are observed by optical microscope, meanwhile the open cavity length and the MZI length are measured as shown in Fig. 6. It should be noted that two red laser are coupled into the FMZI sample, as these propagating red lasers reach to the surface of fabricated micro-cavity

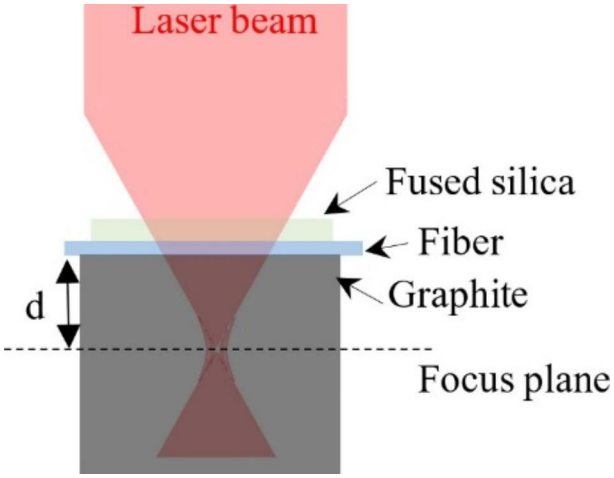

Fig. 5 The experimental scheme for micro-cavity size adjustment

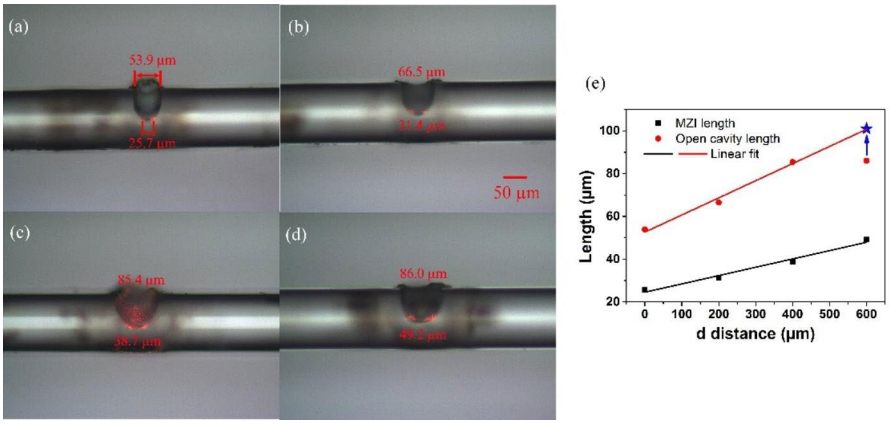

Fig. 6 (a-d) The graphs of FMZI samples observed by optical microscope, the distance *d* between the graphite surface and the focus plane: 0, 200, 400 and 600 μm, respectively. (e) The dependence of lengths on the distance *d*

in the fiber core, obvious red point can be seen due to the light scattering on the surface, thus, the distance between these two red points can be regarded as MZI length approximately.

As shown in Fig. 6(a-d), the size of crater-like structure in fiber increases as *d* distance increases, meanwhile the open cavity length and MZI length also increase, furthermore, MZI length is almost equal to the half of the open cavity length. It should be noted that the open cavity length was measured as 86.0 μm in Fig. 6(d), but was corrected to 101 μm in the same fabrication condition as illustrated in Fig. 2, and the red point is substituted by the blue star in Fig. 6(e). This small discrepancy probably resulted from the different observed direction of the samples. Furthermore, the linearities of the fitted experimental results are quite good in Fig. 6(e). The linear dependence of open cavity length on *d* distance is easily explained by the discussion based on Fig. 5. With regard to the linear dependence of MZI length on *d* distance, we think that as the size of micro-cavity mainly depends on the open

cavity, and the open cavity is determined by the relative distance *d* between the graphite surface and focus plane. So the MZI length is linear related to *d* distance.

As discussed above, the MZI lengths of FMZI are able to be adjusted only by the movement of Z position, meanwhile the fabrication time is not changed, which is superior to the femtosecond laser fabrication system, where the longer MZI length needs longer fabrication time. In addition, in our experiment, the longer MZI length sample was tried to fabricate, however as the laser power is limited (20 W) and the laser beam power is also reduced by the aperture in the optical system, the laser beam power of 14.5 W after aperture is maximum, so longer MZI length sample is not obtained in our case, but we believe that longer MZI length samples are possible with higher power nanosecond laser.

3.2 The refractive index sensing

The optical scheme of FMZI was added in Fig. 7(a), as illustrated, when the propagating light in fiber core meets the micro-cavity, it splits into two paths, one continues in the remained core, the other passes through the removed space of fiber core, these two light paths interfere with each other in fiber core later. In order to confirm the success FMZI fabrication and investigate the sensitivity of samples with different MZI lengths, these samples are utilized to measure the refractive index of ethanol water solution as in the work (Shuhao et al. 2021). For the sample with 25.7 μm MZI length, the transmission spectrum shift is confirmed, but the transmission spectrum dips of solution with refractive index close to water are not shown, thus its transmission spectra and the dependence of resonant wavelength on refractive index is not illustrated in Fig. 7. The experimental and analytical results of other 3 samples with MZI length from 31.4 to 49.2 μm are shown in Fig. 7.

For each FMZI sample, the resonant wavelength of transmission spectrum blue shifts as the refractive index of solution increase as illustrated in Fig. 7(b, d, e), meanwhile, the dependence of resonant wavelength on refractive index shows quite good linearity, which are in good agreement with the work (Shuhao et al. 2021). In addition, the absolute refractive index sensitivities are more than 10,000 nm/RIU, which is comparable with the femtosecond laser fabricated ones (Zhao et al. 2019). In comparison with each other, firstly, for the longer MZI length sample, the free spectrum range becomes shorter and almost one whole period is shown in Fig. 7(f), which is explained by the *Eq. (3)* in Ref. (Shuhao et al. 2021). Secondly, the sensitivity increases as MZI length increases, which seems different with the previous work (Shuhao et al. 2021). However, firstly, the experimental tested refractive index range for different samples are different, the longer MZI length sample tests bigger refractive index range and the absolute refractive index is bigger for more resonant wavelengths are shown in the definite spectrum range (1250–1650 nm); secondly, for the solution with same refractive index, its resonant wavelengths of transmission spectra located at different wavelengths, in particular, in our case, the transmission spectrum of the solution with refractive index 1.336, the resonant wavelengths located at around 1350, 1530 and 1650 nm. From the *Eqs. (2)*&(5) in Ref. (Shuhao et al. 2021), the sensitivity can also be expressed as: $S_{RI} = -\lambda_m/\Delta n_{eff}$. The bigger absolute refractive index results in less Δn_{eff}, the longer located resonant wavelength results in bigger λ_m, these both lead to higher absolute sensitivity. Unfortunately, the resonant wavelength location is not definitely determined and possesses random property; meanwhile, for the definite range of refractive

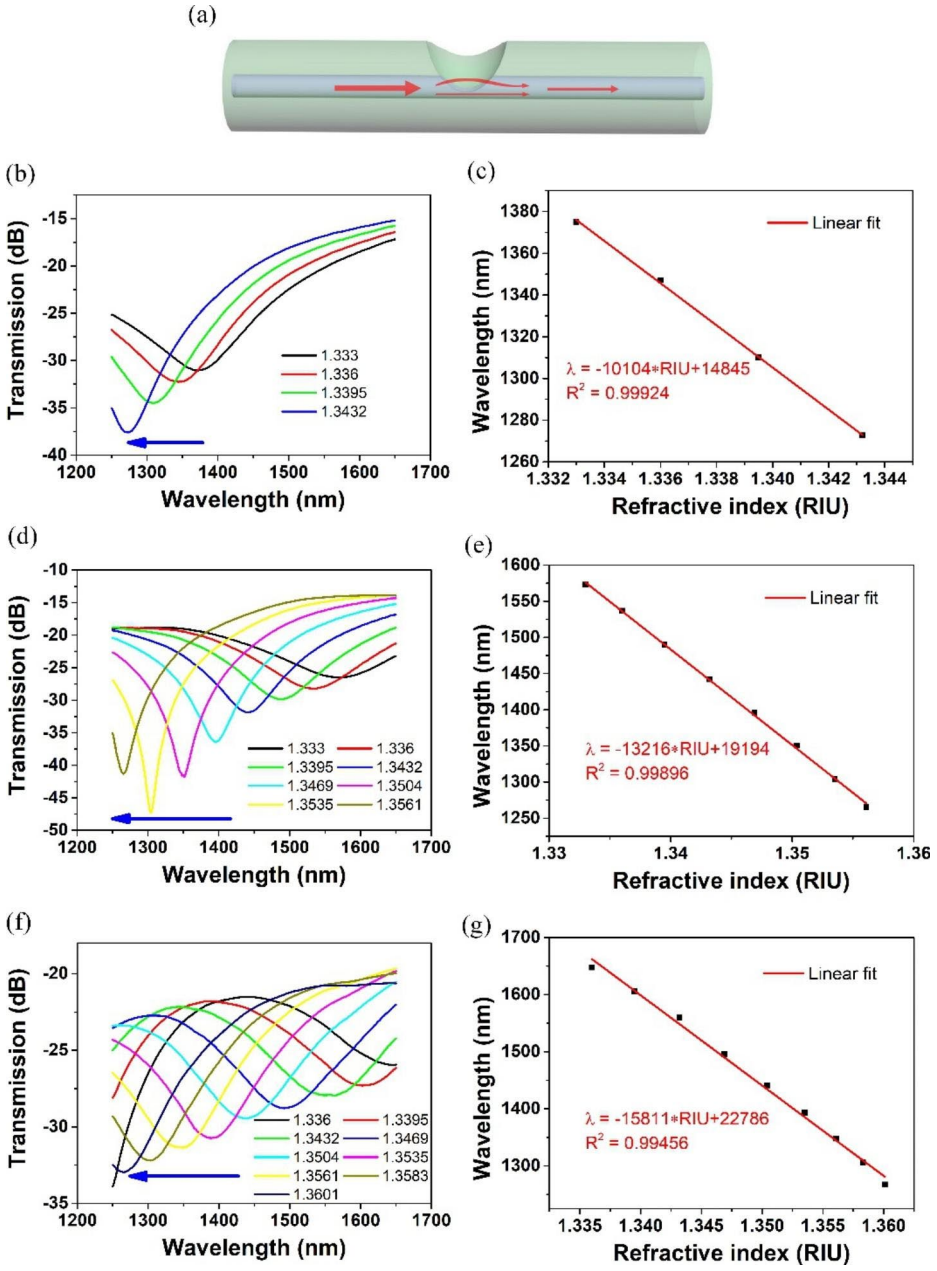

Fig. 7 (a) The optical scheme of FMZI. (b, d, f) Transmission spectra of the fabricated FMZI sensor with MZI length of 31.4, 38.7 and 49.2 μm in different ethanol solutions, respectively. (c, e, g) The resonant wavelength shift vs. the index of ethanol solutions for samples with MZI length of 31.4, 38.7 and 49.2 μm, respectively

index solution, Δn_{eff} should be same. Finally, the sensitivity is not definite related with MZI length as discussed in Ref. (Shuhao et al. 2021).

Regarding to mechanical resistance, if without any protection or fixture, the striped optical fiber is fragile in its mechanical resistance and our fabricated structure weaken its mechanical resistance a lot, leading to the unsuitable for its direct practical application. However, after careful fabrication process, the samples are commonly fixed on glass slide, strengthening its mechanical resistance quite a lot, which makes it suitable for the further tests or applications.

4 Conclusion

In conclusion, we presented the detailed fabrication processes of FMZI by nanosecond laser-induced micro-plasma and its simple micro-cavity size adjustment. The fabrication can be divided into 4 processes: (1) heat transfer, (2) micro-plasma formation, (3) micro-plasma expansion and ablation, (4) cooling down and micro-structure formation. Based on the above understanding, the simple micro-cavity size adjustment is proposed. The MZI length of fabricated FMZI samples possesses linear relationship with the distance between the graphite surface and the focus plane, which is suitable for further production. Meanwhile, compared with the femtosecond laser fabrication method, here only the focus position is needed to be moved. The fabricated FMZI exhibits a high sensitivity of -15,811 nm/RIU (refractive index unit) for the index sensing application.

Acknowledgements The author acknowledges the scholarship from the China Scholarship Council (201306840047). The authors also would like to thank Dr. Wang Dongdong at Nanjing University of Science and Technology, China, for insightful discussions and cordial help in the lab.

Author contributions All authors contributed to the study conception and design. Material preparation, data collection and analysis were performed by Cai Shuhao. The first draft of the manuscript was written by Cai Shuhao, writing - review and editing were performed by Maksim Sergeev, Andrey Petrov, Sergey Varzhel, and Li Li, founding was acquired by Li Li. All authors commented on previous versions of the manuscript. All authors read and approved the final manuscript.

Funding This work is supported by NSAF, China (No. U1830123), and the National Natural Science Foundation of China (No. 61627802).

Data availability No data is available for this work.

Declarations

Competing interests The authors declare no conflicts of interests.

References

Albert, J., Shao, L.Y., Caucheteur, C.: Tilted fiber Bragg grating sensors. Laser Photonics Rev. **7**(1), 83–108 (2013)

Chunyang, H., Hui, D., Xianli, L., Shaofei, D.: Temperature insensitive refractive index sensor based on single-mode micro-fiber Sagnac loop interferometer. Appl. Phys. Lett. **104**(18), 181906 (2014)

Janik, M., Myśliwiec, A.K., Koba, M., Celebańska, A., Bock, W.J., Śmietana, M.: Sensitivity pattern of femtosecond laser micromachined and plasma-processed in-fiber Mach-Zehnder interferometers, as applied to small-scale refractive index sensing. IEEE Sens. J. **17**(11), 3316–3322 (2017)

Jiang, L., Zhao, L., Wang, S., Yang, J., Xiao, H.: Femtosecond laser fabricated all-optical fiber sensors with ultrahigh refractive index sensitivity: modeling and experiment. Opt. Express. **19**(18), 17591–17598 (2011)

Kostyuk, G., Sergeev, M., Zakoldaev, R., Yakovlev, E.: Fast microstructuring of silica glasses surface by NIR laser radiation. Opt. Lasers Eng. **68**, 16–24 (2015)

Li, Z., Liao, C., Wang, Y., Dong, X., Liu, S., Yang, K., Wang, Q., Zhou, J.: Ultrasensitive refractive index sensor based on a Mach-Zehnder interferometer created in twin-core fiber. Opt. Lett. **39**(17), 4982–4985 (2014)

Li, Z., Liao, C., Song, J., Wang, Y., Zhu, F., Wang, Y., Dong, X.: Ultrasensitive magnetic field sensor based on an in-fiber Mach-Zehnder interferometer with a magnetic fluid component. Photonics Res. **4**(5), 197–201 (2016)

Li, Z., Liao, C., Chen, D., Song, J., Jin, W., Peng, G.-D., Zhu, F., Wang, Y., He, J., Wang, Y.: Label-free detection of bovine serum albumin based on an in-fiber Mach-Zehnder interferometric biosensor. Opt. Express. **25**(15), 17105–17113 (2017)

Park, M., Lee, S., Ha, W., Kim, D.-K., Shin, W., Sohn, I.-B., Oh, K.: Ultracompact intrinsic micro air-cavity fiber Mach-Zehnder interferometer. IEEE Photonics Technol. Lett. **21**(15), 1027–1029 (2009)

Rao, Y.-J.: In-fibre Bragg grating sensors. Meas. Sci. Technol. **8**(4), 355 (1997)

Rao, Y.-J., Deng, M., Duan, D.-W., Yang, X.-C., Zhu, T., Cheng, G.-H.: Micro Fabry-Perot interferometers in silica fibers machined by femtosecond laser. Opt. Express. **15**(21), 14123–14128 (2007)

Shuhao, C., Rymkevich, V., Sergeev, M., Samokhvalov, A.: Features of fused silica ablation by laser induced carbon microplasma. Opt. Quant. Electron. **52**(2), 1–11 (2020)

Shuhao, C., Lijing, Z., Sergeev, M., Dmitriev, A., Jiang, Y., Petrov, A., Varzhel, S., Sheng, C., Li, L.: Fiber Mach-Zehnder interferometers fabricated by nanosecond pulses and applications in refractive index sensing.Optics Communications, 127150 (2021)

Sun, X.-Y., Chu, D.-K., Dong, X.-R., Li, H.-T., Hu, Y.-W., Zhou, J.-Y., Duan, J.-A.: Highly sensitive refractive index fiber inline Mach-Zehnder interferometer fabricated by femtosecond laser micromachining and chemical etching. Opt. Laser Technol. **77**, 11–15 (2016)

Tian, Z., Yam, S.S., Loock, H.-P.: Refractive index sensor based on an abrupt taper Michelson interferometer in a single-mode fiber. Opt. Lett. **33**(10), 1105–1107 (2008)

Veiko, V.P., Volkov, S.A., Zakoldaev, R.A., Sergeev, M.M., Samokhvalov, A.A., Kostyuk, G.K., Milyaev, K.A.: Laser-induced microplasma as a tool for microstructuring transparent media. Quantum Electron. **47**(9), 842 (2017)

Wang, Y., Li, Y., Liao, C., Wang, D., Yang, M., Lu, P.: High-temperature sensing using miniaturized fiber inline Mach-Zehnder interferometer. IEEE Photonics Technol. Lett. **22**(1), 39–41 (2009)

Wang, Y.: Review of long period fiber gratings written by CO_2 laser. J. Appl. Phys. **108**(8), 11 (2010)

Wei, T., Han, Y., Tsai, H.-L., Xiao, H.: Miniaturized fiber inline fabry-perot interferometer fabricated with a femtosecond laser. Opt. Lett. **33**(6), 536–538 (2008)

Zhao, L., Jiang, L., Wang, S., Xiao, H., Lu, Y., Tsai, H.-L.: A high-quality Mach-Zehnder interferometer fiber sensor by femtosecond laser one-step processing. Sensors. **11**(1), 54–61 (2011)

Zhao, Y., Zhao, H., Lv, R., Zhao, J.: Review of optical fiber Mach-Zehnder interferometers with micro-cavity fabricated by femtosecond laser and sensing applications. Opt. Lasers Eng. **117**, 7–20 (2019)